

1 Fast-get-faster explains wavier upper-level jet stream under
2 climate change

3 Tiffany Shaw^{1*}, Osamu Miyawaki², Hsing-Hung Chou¹, Russell Blackport³

4 ^{1*}Department of the Geophysical Sciences, The University of Chicago, Chicago, IL, USA.

5 ²Climate and Global Dynamics Laboratory, National Center for Atmospheric Research,
6 Boulder, CO, USA.

7 ³Canadian Centre for Climate Modelling and Analysis, Environment and Climate
8 Change Canada, Victoria, BC, Canada.

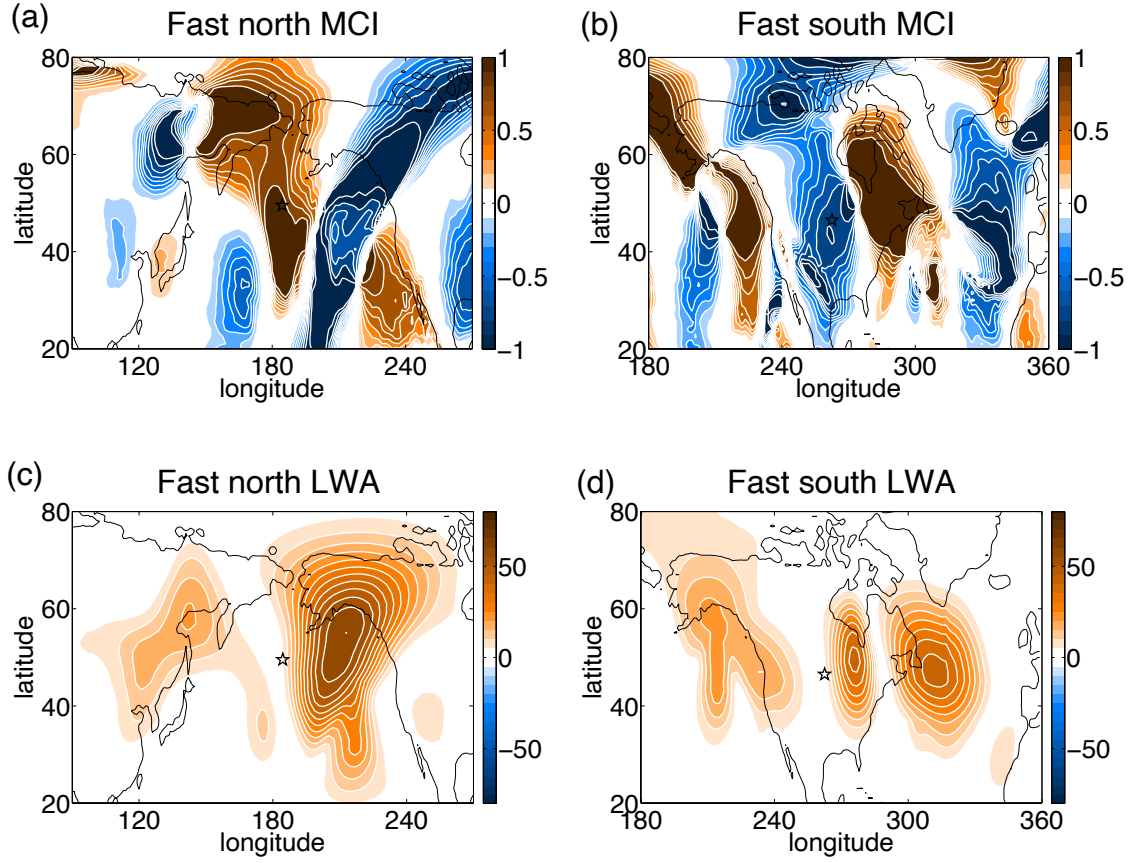
9 *Corresponding author(s). E-mail(s): tas1@uchicago.edu;

Supplementary Table 1: CMIP6 models analyzed in this study.

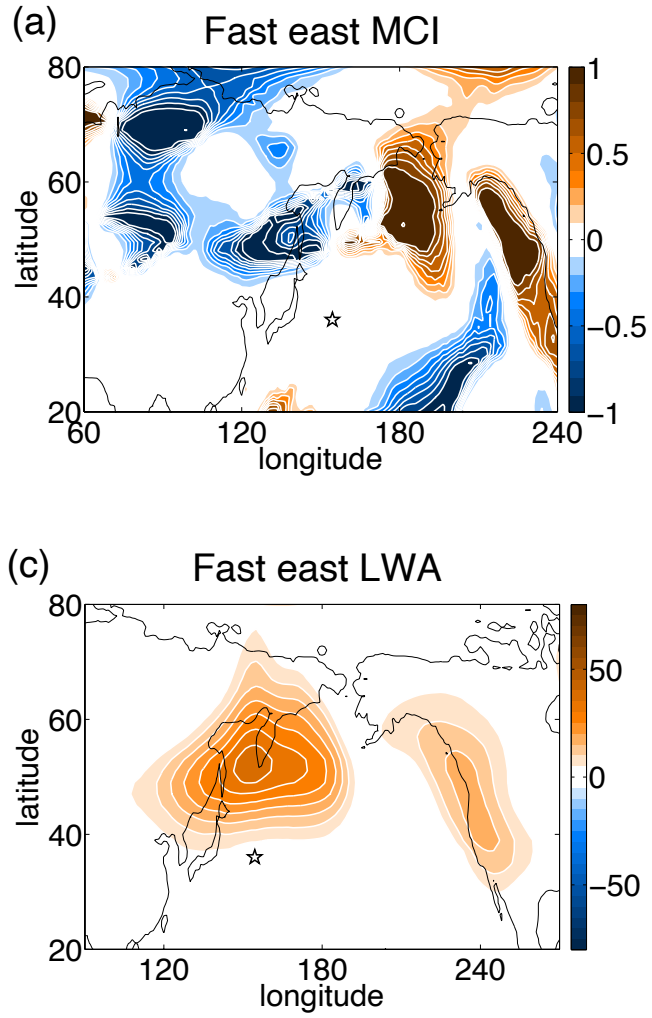
<i>Model</i>	<i>realization</i>	<i>scenario</i>
ACCESS-CM2	rli1p1fl	historical, SSP5-8.5
BCC-CSM2-MR	rli1p1fl	historical, SSP5-8.5, amip, amip-p4K
CanESM5	rli1p1fl	historical, SSP5-8.5
CESM2-WACCM	rli1p1fl	historical, SSP5-8.5, amip, amip-p4K, aqua, aqua-p4K
FGOALS-g3	rli1p1fl	historical, SSP5-8.5
GFDL-CM4	rli1p1fl	historical, SSP5-8.5
IITM-ESM	rli1p1fl	historical, SSP5-8.5
INM-CM4-8	rli1p1fl	historical, SSP5-8.5
INM-CM5-0	rli1p1fl	historical, SSP5-8.5
IPSL-CM6A-LR	rli1p1fl	historical, SSP5-8.5, amip, amip-p4K, aqua, aqua-p4K
KACE-1-0-G	rli1p1fl	historical, SSP5-8.5
MIROC6	rli1p1fl	historical, SSP5-8.5, amip, amip-p4K, aqua, aqua-p4K
MPI-ESM1-2-LR	rli1p1fl	historical, SSP5-8.5
MPI-ESM1-2-HR	rli1p1fl	historical, SSP5-8.5
MRI-ESM2-0	rli1p1fl	historical, SSP5-8.5, amip, amip-p4K, aqua, aqua-p4K
NorESM2-LM	rli1p1fl	historical, SSP5-8.5
NorESM2-MM	rli1p1fl	historical, SSP5-8.5
TaiESM1	rli1p1fl	historical, SSP5-8.5, amip, amip-p4K, aqua, aqua-p4K

Supplementary Table 2: Arctic Sea ice loss simulations analyzed in this study taken from Kang et al. (2023). PAMIP output from pdSST-pdSIC and pdSST-futArcSIC where pdSIC and futArcSIC impose present-day sea ice and sea ice loss under 2C warming, respectively.

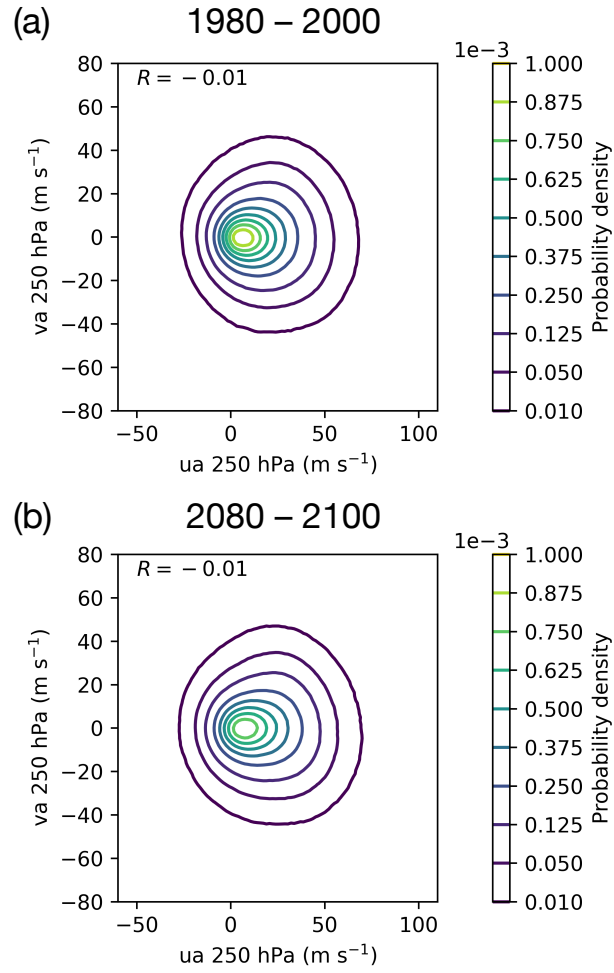
<i>Model</i>	<i>PAMIP</i>	<i>years</i>	<i>ensemble members</i>
WACCM4 coupled	no	200	1
WACCM4 uncoupled	no	200	1
AWI-CM-1-1-MR	yes	1	100
CanESM5	yes	1	200
CESM2	yes	1	200
HadGEM3-GC31-MM	yes	1	300
IPSL-CM6A-LR	yes	1	200
MIROC6	yes	1	100



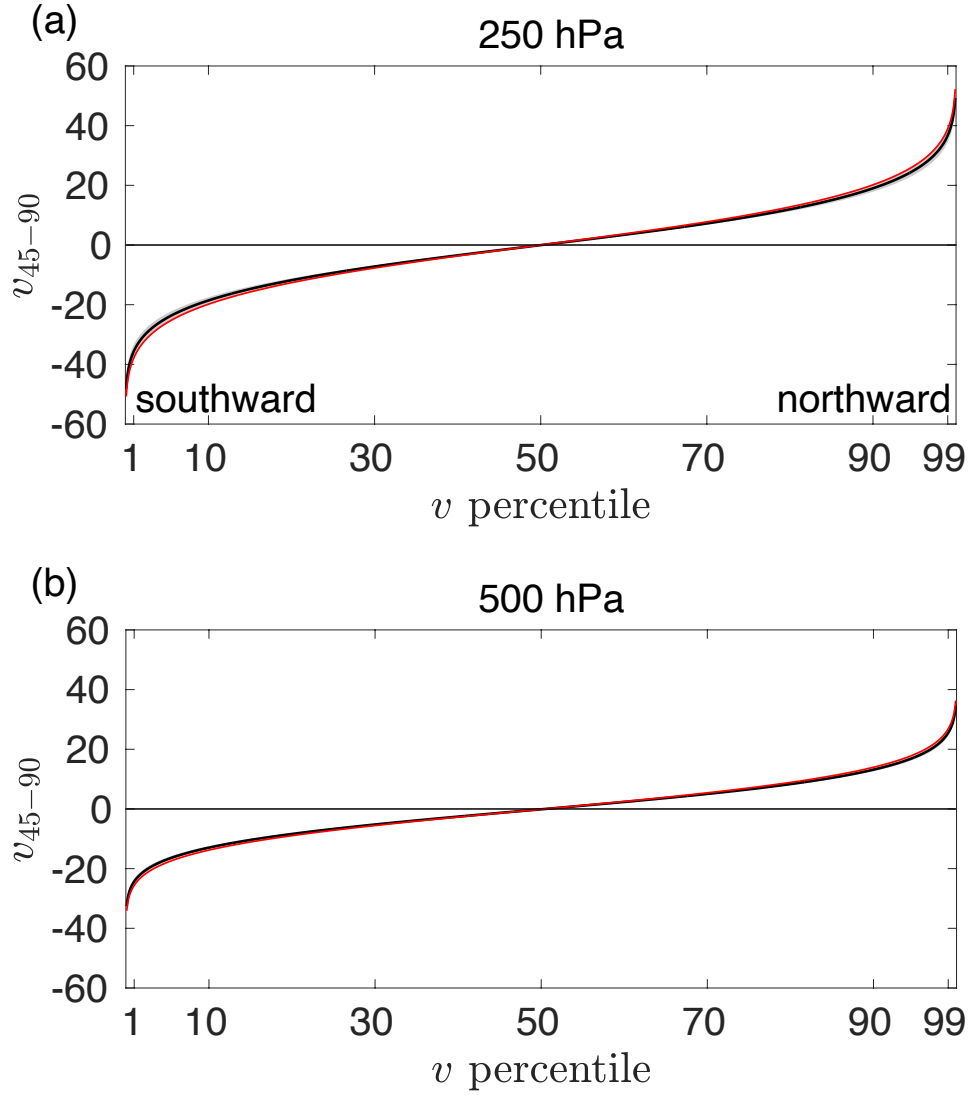
Supplementary Fig. 1: Fast upper-level jet stream wind. Example of Meridional circulation index for fast (a) northward and (b) southward wind at location indicated by the black star. (c,d) Similar to (a,b) but for Local Wave Activity (divided by 10^9 m^2).



Supplementary Fig. 2: Fast upper-level jet stream wind. Example of (a) Meridional circulation index and (b) Local Wave Activity (divided by 10^9 m^2) for fast eastward wind at location indicated by the black star.

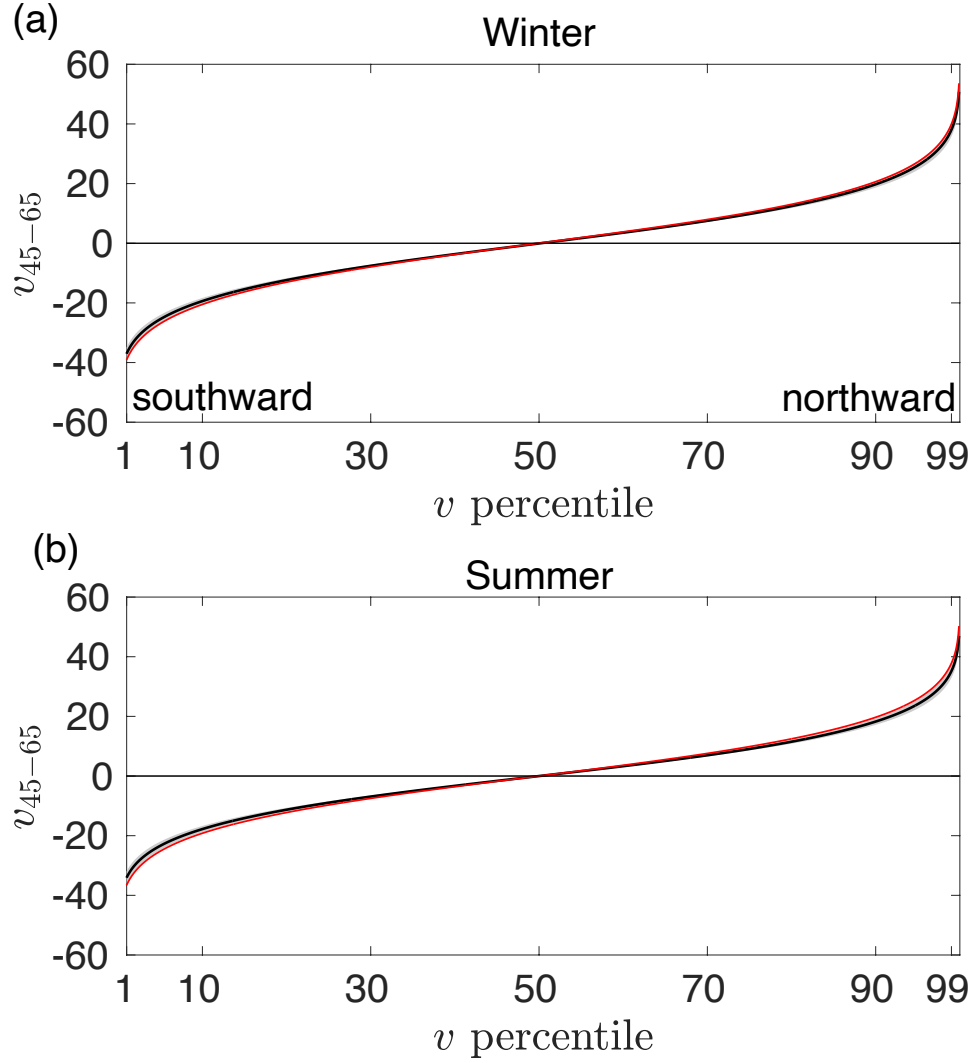


Supplementary Fig. 3: Relationship between fast eastward and meridional upper level jet stream wind distributions. Extratropical ($45\text{--}90^\circ$) upper level 250 hPa east-west versus north-south jet stream wind for each day and spatial location for (a) 1980-2000 and (b) 2080-2100.

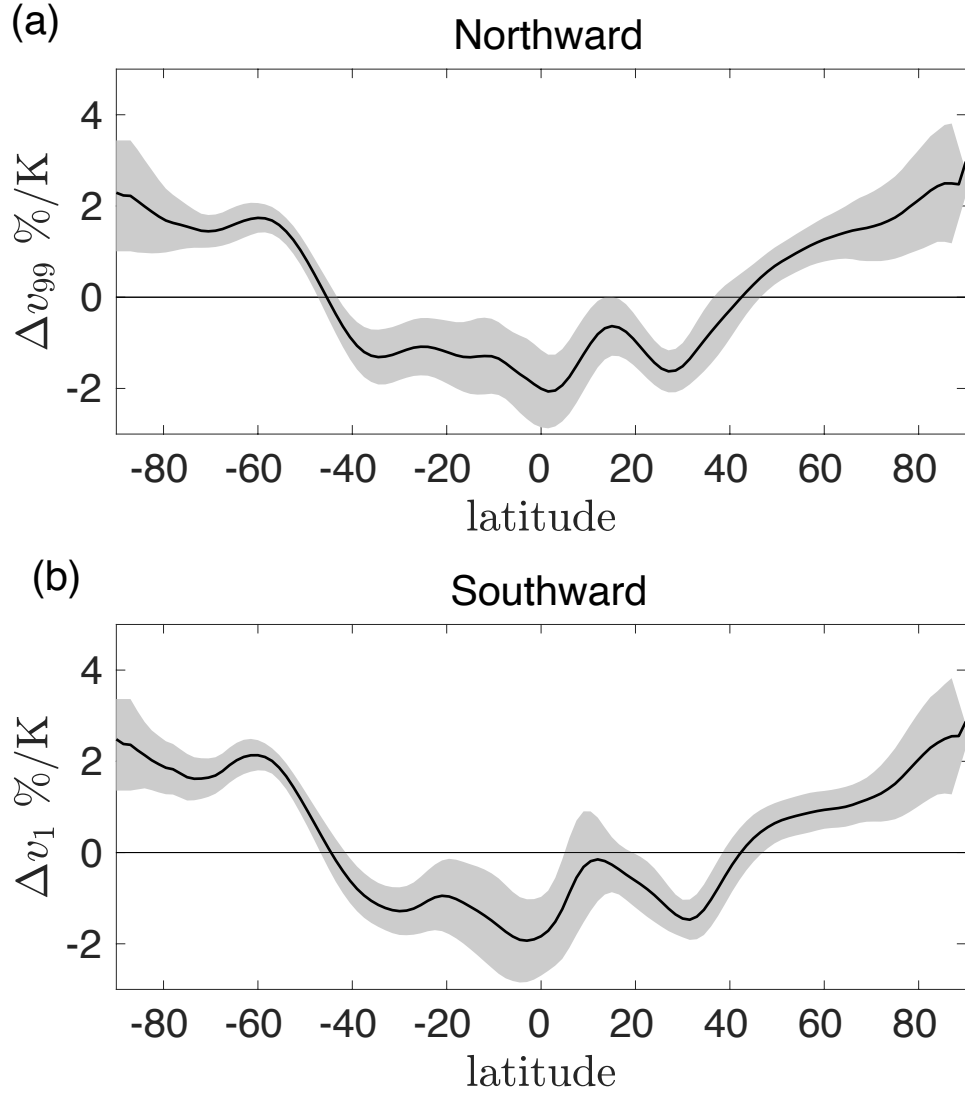


Supplementary Fig. 4: Meridional wind distribution in reanalysis data and climate models.

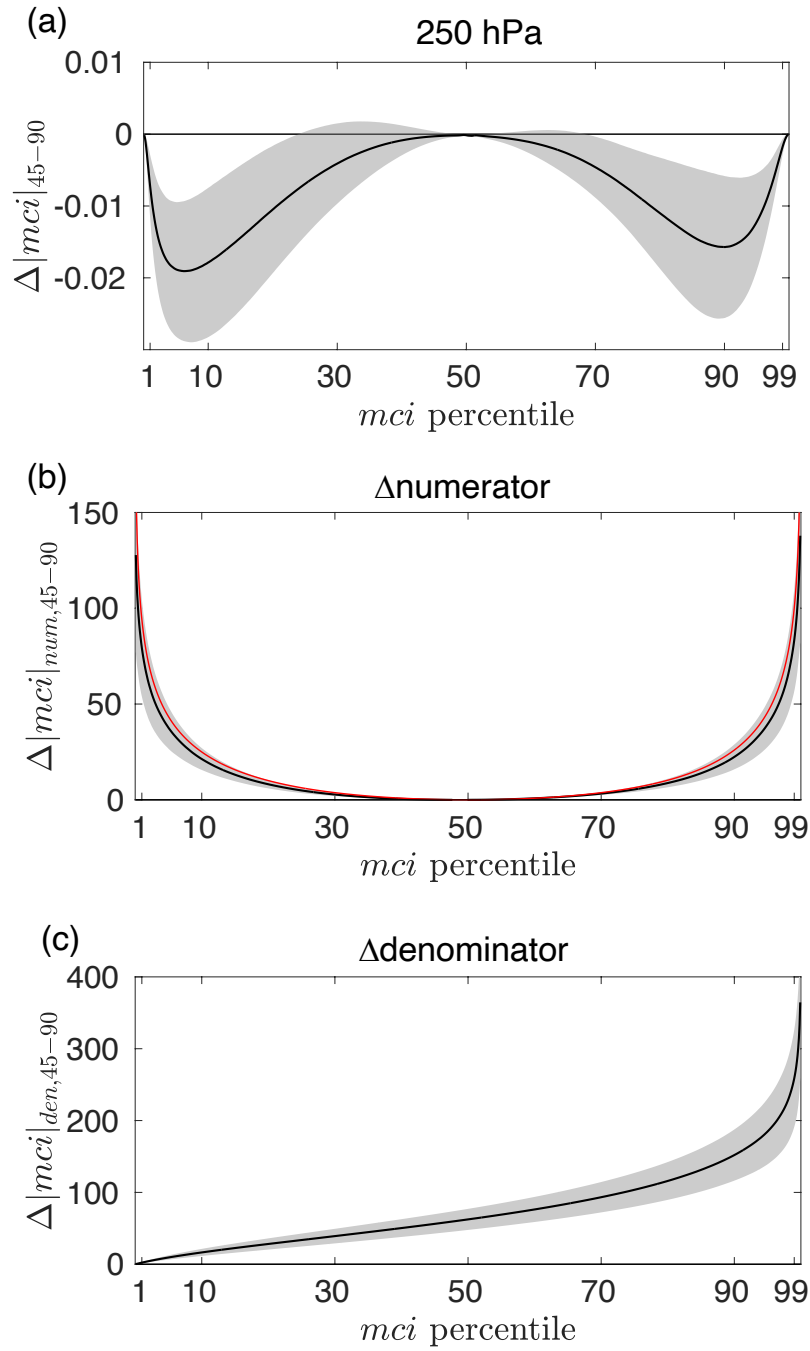
Extratropical ($45-90^\circ$) jet stream waviness distribution at (a) 250 hPa and (b) 500 hPa in reanalysis data (red) and coupled climate models (black) in the late 20th century (1980-2000). Shading indicates one standard deviation of the response across the model ensemble.



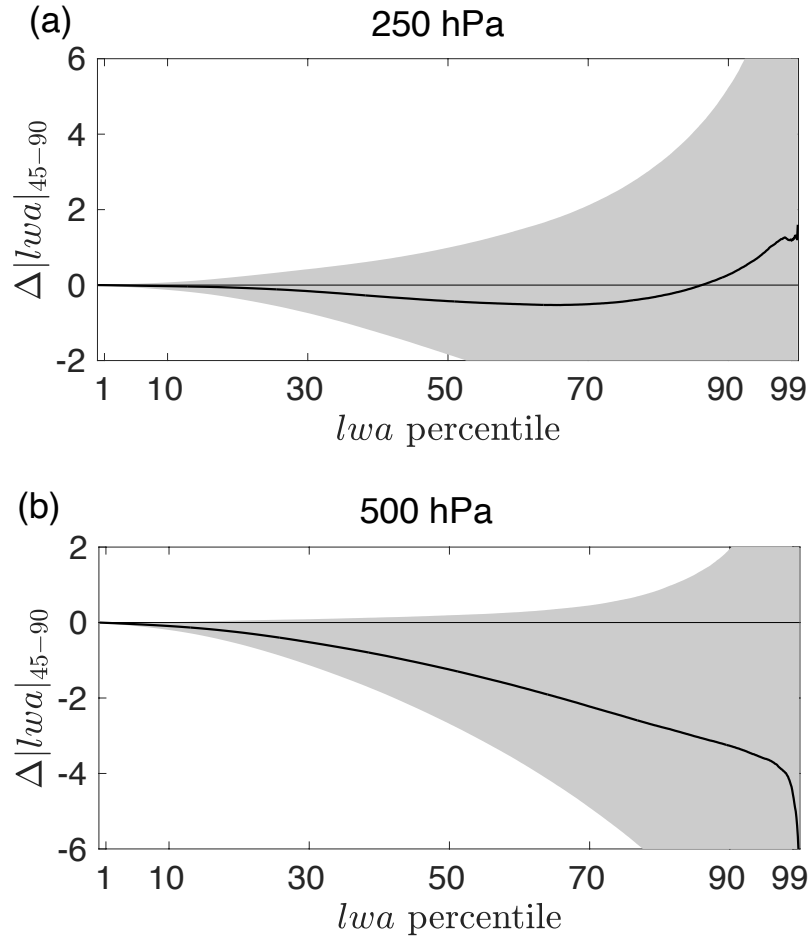
Supplementary Fig. 5: Seasonality of upper-level meridional wind distribution in reanalysis data and climate models. Extratropical ($45-90^\circ$) jet stream waviness distribution at 250 hPa in reanalysis data (red) and coupled climate models (black) during (a) winter (October to March in the Northern Hemisphere and April to September in the Southern Hemisphere) and (b) summer (April to September in the Northern Hemisphere and October to March in the Southern Hemisphere) in the late 20th century (1980-2000). Shading indicates one standard deviation of the response across the model ensemble.



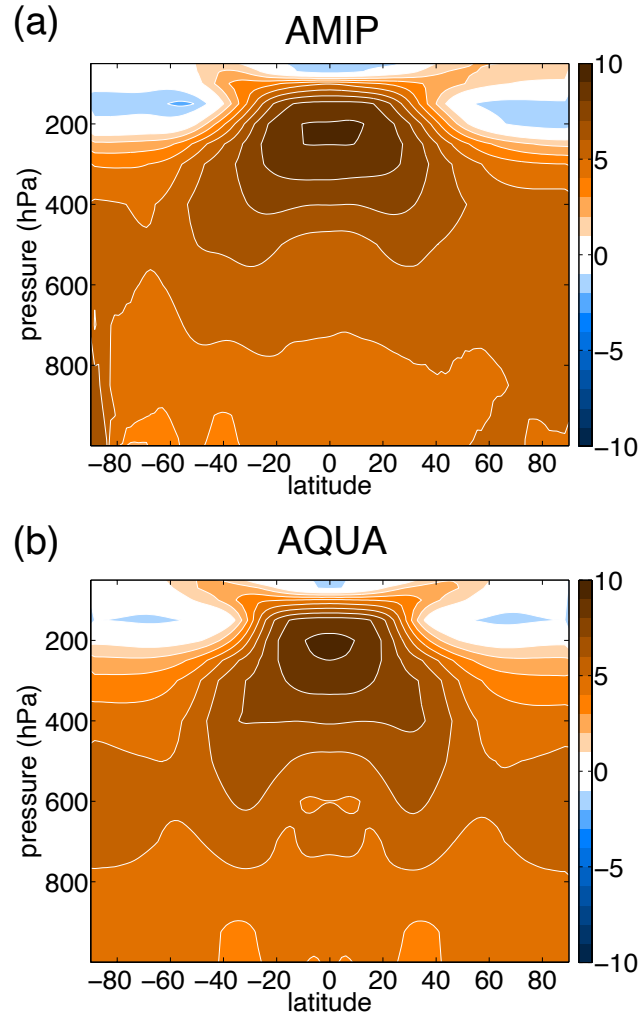
Supplementary Fig. 6: Extreme northward and southward meridional wind under climate change. Fractional changes in the extreme (a) northward (> 99th percentile) and (b) southward (< 1st percentile) of the upper-level (250 hPa) waviness distribution normalized by the global mean surface warming for each model. Shading indicates one standard deviation of the response across the model ensemble.



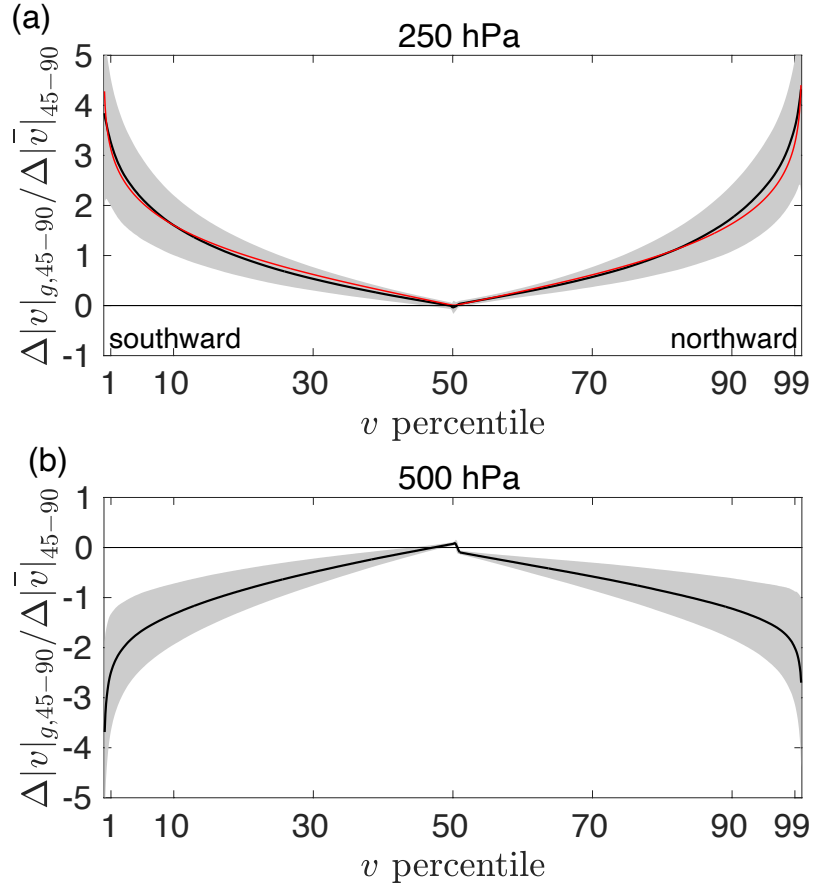
Supplementary Fig. 7: Meridional circulation index under climate change. Response of the meridional circulation index distribution in the extratropics (45–90°) at (a) 250 hPa. The response of the numerator and denominator of the MCI are shown in (b) and (c) respectively. The red line indicates the prediction following an increase of 2% per degree of surface air temperature change times the late 20th century distribution.



Supplementary Fig. 8: Local Wave Activity under climate change. Response of Local Wave Activity distribution in the extratropics (45–90°) at (a) 250 hPa and (b) 500 hPa. Values have been divided by 10^6 m^2 .

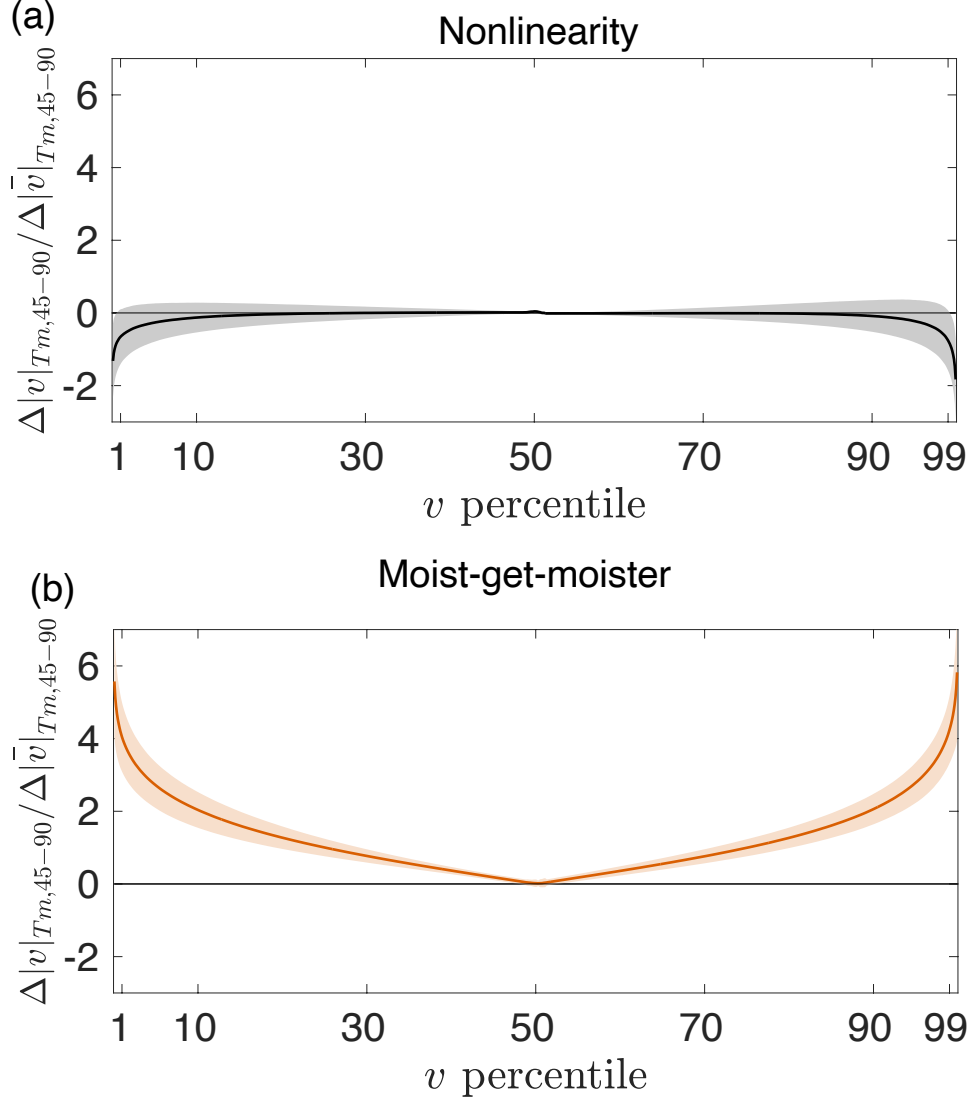


Supplementary Fig. 9: Temperature response in idealized configurations. Zonal-mean temperature response to + 4 K sea surface temperature increase in (a) atmosphere-only and (b) aquaplanet models (contour interval is 1 K).

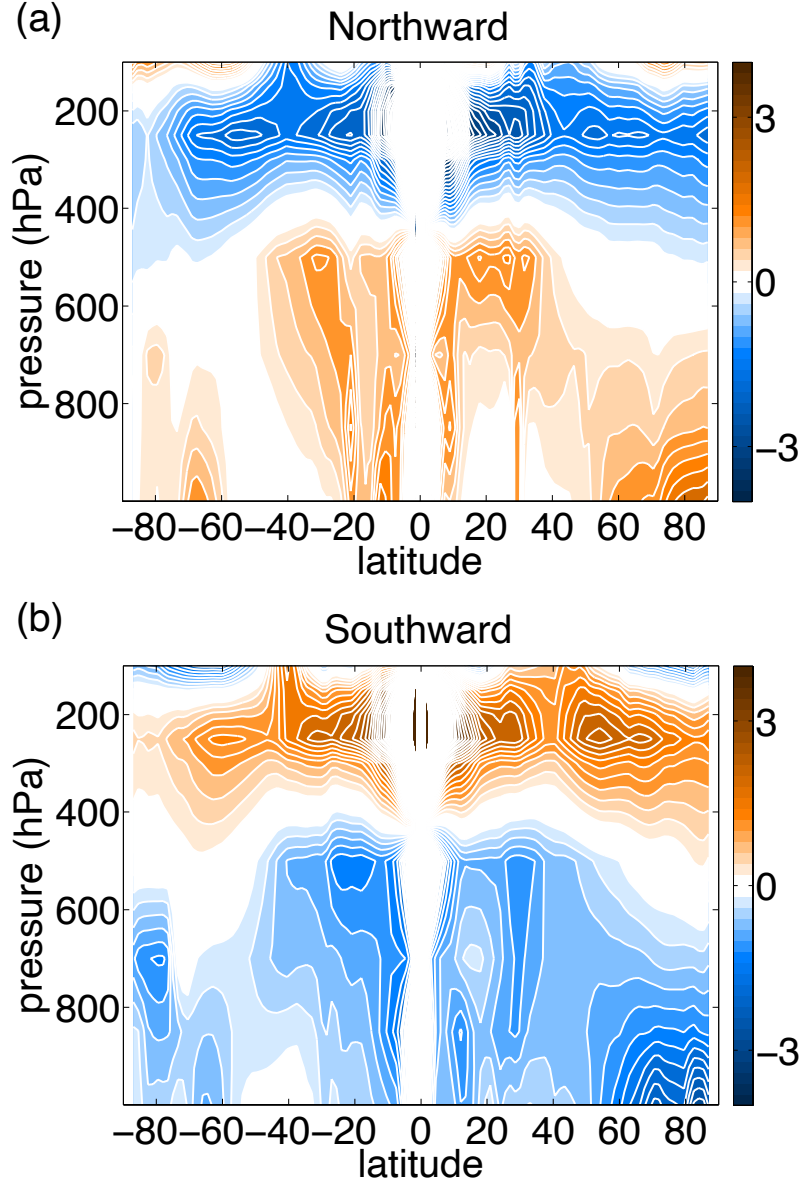


Supplementary Fig. 10: Meridional geostrophic jet stream winds under climate change.

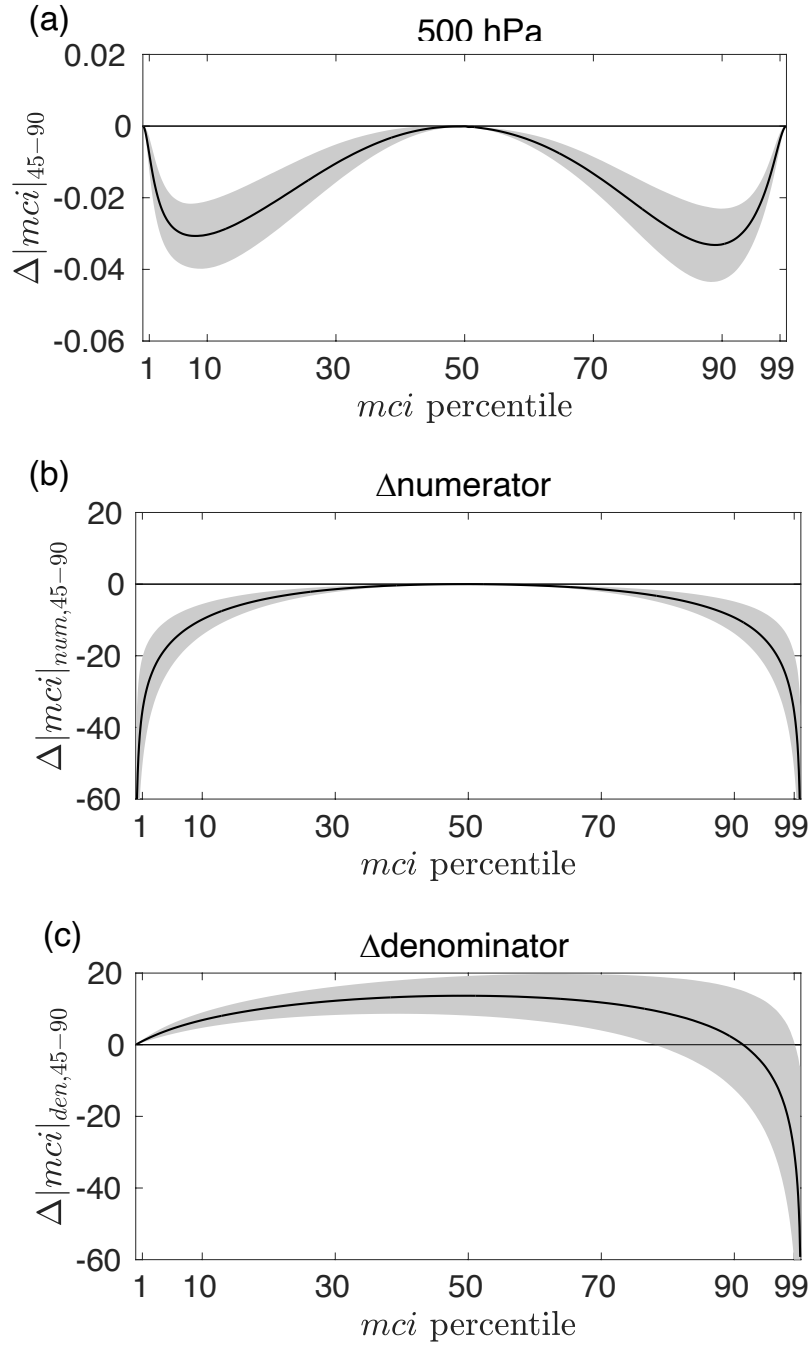
Response of the extratropical (45–90°) geostrophic waviness (meridional geostrophic wind) distribution at (a) 250 hPa and (b) 500 hPa in both hemispheres across percentiles relative to the response of average waviness (\bar{v}). Shading indicates one standard deviation of the response across the model ensemble. The red line indicates the prediction following an increase of 2% per degree of surface air temperature change times the late 20th century distribution.



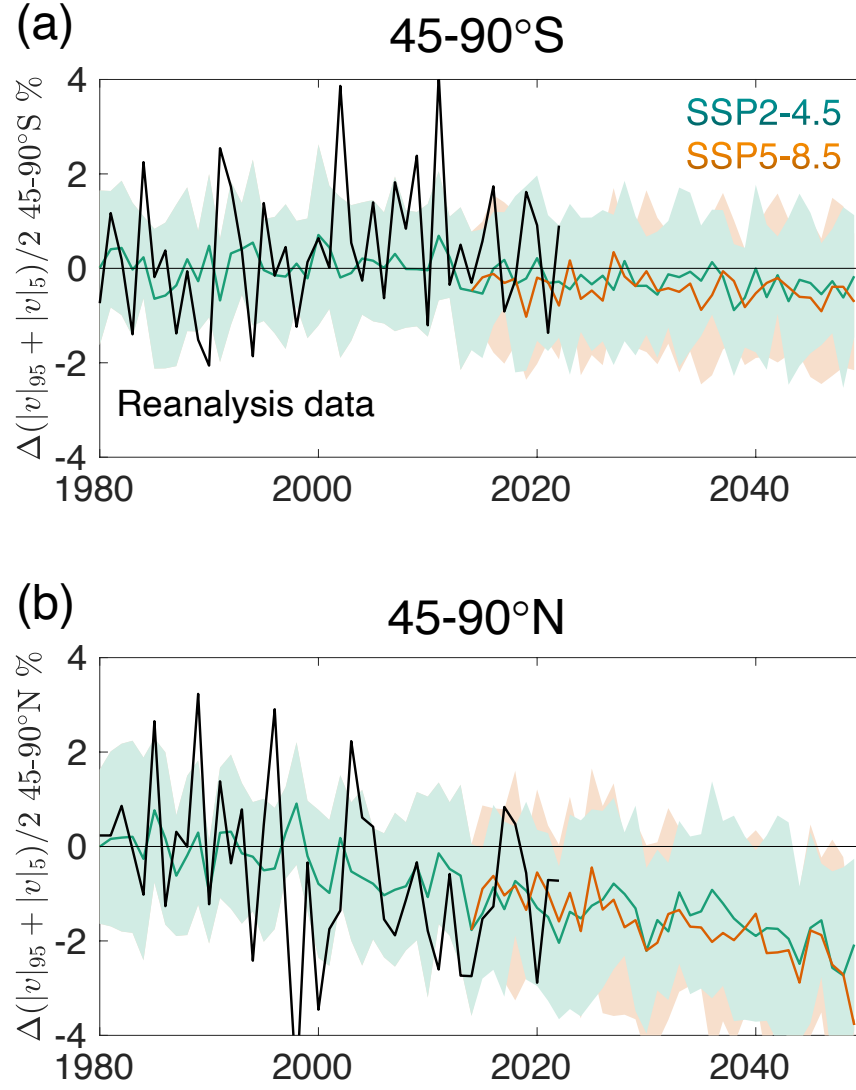
Supplementary Fig. 11: Moist thermal wind decomposition of fast-get-faster response of upper-level waviness. (a) Residual of extratropical (45–90°) moist thermal wind decomposition at 250 hPa in both hemispheres across percentiles relative to the response of average waviness (see equation 4 in main text). (b) Response of upper-level moist thermal wind over the extratropics (45–90° latitude) in both hemispheres across percentiles relative to the response of the average wind (\bar{v}_{Tm}) due to the moist-get-moister contribution without any change in longitudinal temperature gradient (see equation 5 in main text).



Supplementary Fig. 12: Relationship between wavy-get-wavier response and moisture under climate change. Latent heat release contribution to the fractional changes in extreme (a) northward (> 99 th percentile) and (b) southward (< 1 st percentile) moist thermal wind, i.e. the sum of the first and second term in the integrand of equation (4) multiplied by $-1/(fa \cos \phi)$ (contour interval is $200 \text{ m}^2 \text{ s kg}^{-1}$).



Supplementary Fig. 13: Meridional circulation index under climate change. Response of the meridional circulation index distribution in the extratropical (45–90°) at (a) 500 hPa. The response of the numerator and denominator of the MCI are shown in (b) and (c) respectively.



Supplementary Fig. 14: Emergence of mid-level waviness signal. Time series of fractional changes (relative to the 1980-2000 period) in extreme northward and southward (95th and 5th percentile) mid-level (500 hPa) waviness in reanalysis-mean (black line) and climate models for different emission scenarios (colored lines) for the (a) Southern and (b) Northern Hemisphere extratropics in the satellite era (1980-2022). Shading indicates one standard deviation across the model ensemble.